*Korean J. Chem. Eng.*, 40(5), 1141-1150 (2023)
DOI: 10.1007/s11814-022-1341-7

pISSN: 0256-1115
eISSN: 1975-7220

# Thin film composite on sulfonated PVDF electrospun and its performance in nanofiltration

**Omid Qanati, Zahra Dusti, Mir Saeed Seyed Dorraji†, Arsalan Ahmadi, and Mohammad Hossein Rasoulifard**

Applied Chemistry Research Laboratory, Department of Chemistry, Faculty of Science, University of Zanjan, Zanjan, Iran
(*Received 12 May 2022 • Revised 28 October 2022 • Accepted 6 November 2022*)

**Abstract**−Thin-film composite membranes (TFC) have attracted great attention in the field of seawater and wastewater treatment. A novel nanofiltration membrane was fabricated via interfacial polymerization of meta phenylene diamine (MPD) and 1,3,5-benzene tricarbonyl chloride (TMC) on the surface of a recently developed nanofibrous mat from sulfonated PVDF (S-PVDF). Chlorosulfonic acid was used to sulfonate PVDF powder, and new peaks on $^1$HNMR and FT-IR techniques confirmed the preparation of S-PVDF. Using solutions of NaCl, $CaCl_2$, $MgSO_4$, and $Na_2SO_4$, a filtration trial was performed with dead-end filtration equipment. The results demonstrated that sulfonation of PVDF decreased the water contact angle from 137.1 for intact PVDF to 85.5 for S-PVDF/PVDF (50/50). In addition, it reduced the mean diameter of nanofibers from 300 to under 130 nm and, consequently, smaller pores with a mean size of around 90 nm were formed. The membrane containing 10% S-PVDF had the highest steady pure water flux by 25.5 L/m$^2$h and exhibited higher rejection of bivalent and univalent salt ions (>97% bivalent and >88% univalent) with the sensible flow. The electrospun nanofibrous S-PVDF/PVDF proved to be a usable supporting material with a higher hydrophilic character that makes electrospun mats an interesting option for liquid treatment.

Keywords: Sulfonated PVDF, Nanofiltration, Electrospinning, Composite Membrane, Interfacial Polymerization

## INTRODUCTION

In many sciences and industries, separation processes are of particular importance. Natural raw materials are usually a set of different components. In addition, to perform industrial activities, it is often necessary to separate different components of the raw materials and use each one optimally. In addition, industrial products often need to be separated and purified, and if no excess materials are separated, product quality will suffer. Today, a wide range of separation processes is available. The most widely used traditional separation methods are evaporation, distillation, various types of crystallization, etc. During the last decades, membrane technologies have been associated with old separation methods because of their ease and high efficiency, and in some cases have even been used as the main separation process. Membranes, as the main separation agent in these processes, are permeable or semi-permeable phases that prevent the penetration or passage of certain particles. Membrane selectively allows some materials in one phase to pass through to another [1]. Four main factors have prevented the widespread use of membranes in separation processes: unreliability, slow speed, unselectability, and high cost. Various solutions for each of these problems have been proposed over the past 40 years, and the application of membranes in separation processes is very common today. The Loeb-Sourirajan process in the early 1960s enabled us to produce asymmetric reverse osmosis membranes with high permeability [2]. These membranes consist of a very thin layer with high selectivity, which is placed on micro-porous layers with a higher thickness and very high permeability. This thick layer acts as a mechanical reinforcement. Non-porous membranes can separate even particles of approximately equal size. In non-porous membranes, the intrinsic properties of the membrane-forming polymer affect the selectivity and permeability of the membrane [3]. Electrospinning is a simple technique that is known as one of the best methods for producing nanofibers. This technique, first reported by Farmhall in 1934, uses an electric charge to control the formation of polymer fibers on the target body [4]. Various polymer solutions are used in this technique, which can be biodegradable, non-biodegradable, natural materials, or mixtures of these polymers [5]. Nanofibers from electrospinning are suitable for a wide range of applications. The porous structure and wide surface area of these fibers make them ideal for filtering sub-micron particles in water or air. In addition, with the spinning technique, nanostructured scaffolds can be prepared on which different cell cultures are performed [6-8]. Nanofiltration is known as gentler reverse osmosis since it has bigger membrane holes than reverse osmosis membranes. Because these membranes work at quite lower pressures and pass through some inorganics, nanofiltration can be used in situations where high elimination of organic matter is needed as well as in moderate removal of inorganics. This procedure can extract sugar, bivalent salts, and proteins. Its benefit over reverse osmosis is that nanofiltration ordinarily works at higher yields, thus saving total water usage. Yet, this method is not successful for low molecular weight organic compounds such as methanol. Nanofiltration has generated optimal conditions in terms of energy charge and ion repellency and pore width, among other procedures [9]. Interfacial polymerization membranes are widely used in nanofiltration and reverse osmosis except for gas separation (due to swelling of the hydrogel filling in the base membrane cavities in water). One

†To whom correspondence should be addressed.
E-mail: dorraji@znu.ac.ir

of the most important methods of preparing nanofiltration membranes is the polymerization method in the joint chapter, which was innovated by John Cadet. The reverse osmosis membranes obtained by this method are much more efficient than the asymmetric membranes made by the phase change method of salt repulsion and water flow [10]. In this method, due to the polymerization reaction between two very active monomers at the connection of two non-mixing solutions, a very thin film is formed on a porous substrate. In the first stage, the substrate, usually a porous membrane (such as ultrafiltration or microfiltration membranes), is dipped in a water-based solution enclosing an active monomer or a prepolymer such as an amine. This causes the said monomer to sink into the pores of the porous substrate (polysulfone is commonly used as the substrate). The membrane is dipped in a second solution including another active monomer such as hydrochloric acid (acyl halide). These two monomers react together at the interface of the two solutions to form a very thin and dense polymer layer. The advantage of this method is that the reaction stops automatically; because of performing the polymerization reaction in the joint of two solutions and creating a thin polymer layer, the movement of other monomers to each other and the reaction is prevented and the created polymer layer acts as a barrier against the next steps of the polymerization reaction. The resulting polymer layer is very thin, about 100 nanometers. Diamine is in the water-based solution and chloride is in the organic solution, and the reaction takes place between an aqueous phase and an organic phase. The thin layer that is created by this method on the surface of the substrate membrane is a polymer that has many transverse bonds and its thickness is very small, in the range of 0.1 microns or less. For this reason, the permeability of this composite membrane is high. The existence of high cross-links also causes the selectivity of composite membranes made by this method to be high. Beneath this surface layer, a layer of colloidal gel is formed with fewer transverse bonds and much greater permeability, and to some extent fills the pores of the porous substrate. Although the resulting polymer layer determines the selectivity of the membrane, the porous nature of the substrate also strongly affects the membrane flux. The composite membranes made by this method are widely used in reverse osmosis and nanofiltration processes. Among the types of polymers, polyvinylidene fluoride as a polymer with high thermal stability, good chemical resistance against the attack of factors such as organic solvents and acids and bases, is extensively used as an optimal support polymer [11]. Recently, the use of electrospun nanofibers as a protective layer due to their unique properties such as high porosity, interconnected pore structure, and high water permeability, has attracted the attention of researchers around the world [12]. Because electrified nanofibers have a relatively large diameter distribution, they are difficult to use to make nanofiltration membranes and it is difficult to fabricate an integrated thin-film about 100 nm thick on a large pore-sized protective layer [13, 14]. To solve this problem, Xiao et al. electrified a thin layer of copolymerized polyacrylonitrile nanofibers with acrylic acid. This layer has a covalent bond due to having carboxyl groups with a very thin polyamide layer, and this has caused the polyamide thin layer to have an integrated and flawless structure [15]. In 2013, Wang and his colleagues changed the electrospinning conditions to provide different supports in terms of fiber diameter, pore size, and surface roughness and synthesized a thin polyamide film on them using TMC and MPD. They observed that as the fiber diameter decreased, which led to a reduction in pore size, the thickness of the polyamide film increased and the flux decreased. This suggests that the different morphology of the support causes differences in the thin film structure and affects membrane performance [16]. If the support is hydrophobic, such as polyvinylidene fluoride, the selector thin layer cannot stick well to it [9]. One of the main approaches to overcome this problem is making the support hydrophilic. The types of supports can be used with functioning or adding water-like nanoparticles. In recent researches, different corrective techniques have been utilized to enhance the performance of membranes. One of these methods is to use nanoparticles in the structure of membranes. To improve the performance of membranes, nanoparticles such as silicon oxide, titanium oxide, multi-carbon nanotubes walls, and zeolites have been added into the thin layer, causing to improve flux, stability, and effective separation [17]. Vatanpour et al. in 2015 prepared nanofiltration membranes based on polysulfone by embedding multi-walled carbon nanotubes functioned with amine groups in the texture of the membrane, and they observed a significant increase in the membrane performance [18]. In 2007, Barona et al. used chlorosulfonic acid to charge a commercial microfiltration PVDF membrane and performed tests on charged polystyrene sulfonic acid (PSSA) molecules. The results showed that pure water flux increased with an increasing degree of sulfonation, and membrane clogging decreased under the same conditions [19]. The present study aimed to create a very thin integrated and flawless polyamide layer with high performance on the surface of microporous support from sulfonated polyvinylidene fluoride/polyvinylidene fluoride (S-PVDF/PVDF) Using the S-PVDF/PVDF blend introduces groups of sulfonic acid onto the surface of the support layer and significantly increases the thin film composite adhesion to it. This novel support layer makes it easier to form a thin layer and eliminates the need to use techniques such as reverse interfacial polymerization. For this purpose, (S-PVDF/PVDF) electrospun mats with different percentages were used as a support layer and the effect of changing the hydrophilicity and diameter of the fibers on the performance of the composite membrane was investigated. A very thin layer of polyamide (resulting from the reaction of methanephylenediamine as the aqueous phase monomer and 1,3,5-benzene tricarbonyl chloride as the organic phase monomer under the interfacial polymerization process) was then formed on it.

## EXPERIMENTAL

### 1. Materials

Polyvinylidene fluoride (PVDF) powder (Mw≂37×104 g/mol) was obtained from Aldrich Chemicals. N, N-Dimethylformamide (DMF, 99.8%), 1, 2-dichloroethane (99.5%), chlorosulfonic acid (97%), and isopropyl alcohol (99.5%), Triethylamine (40% in water), acetone (99.5%), meta phenylene diamine (MPD), 1,3,5-benzene tricarbonyl chloride (TMC), NaCl, $CaCl_2$, $MgSO_4$, $Na_2SO_4$, and LiCl were all supplied from Merck (Germany). Non-woven Hollytex 3329 was purchased from Kavon filter products Co., USA.

**Table 1. The electrospinning conditions**

| Applied voltage (kV) | Flow rate (ml/h) | Needle to collector distance (cm) | Rotating speed (rpm) | Ambient temperature | Inner diameter of needle (mm) |
|---|---|---|---|---|---|
| 22 | 1 | 15 | 300 | 27-29 | 0.337 |

**2. Sulfonation of PVDF (S-PVDF)**

Chlorosulfonic acid is one of the most potent agents and is preferably used for the sulfonation of polymers [21-24]. PVDF was sulfonated using the procedure reported in the literature. 1 g of PVDF powder and 5 ml chlorosulfonic acid were blended in a clean glass flask under uninterrupted thrilling 500 rpm at 80 °C in an oil bath for 45 min. Finally, the consequent blend was precipitated with 1, 2- dichloroethane and afterward in deionized water. The resulting black precipitate was rinsed several times with 1, 2-dichloroethane as well as deionized water. The sulfonated PVDF powder was dehydrated in an oven at 80 °C for 12 h. After drying, the dark brown precipitate gathered.

**3. Polymer Characterization**

Fourier transform infrared spectroscopy was used to confirm the formation of the sulfonic acid functional group on the polyvinylidene fluoride polymer chain. $^1$H NMR spectrum was obtained using a Bruker 250 MHz spectrometer in d6-dimethylsulfoxide (d6-DMSO) as the solvent-polymer at room temperature. Tetramethylsilane (TMS) was utilized as the internal standard chemical shift reference.

**4. Preparation of Support Layer by Electrospinning Process**

Based on our previous study [20], a solution of DMF and acetone with a volume ratio of 3 : 2 was prepared; consequently, four different solutions were prepared using 0.01% of LiCl and 8% of S-PVDF/PVDF mixture with the following weight ratio: 0/100, 10/90, 30/70, and 50/50. The obtained solutions were thrilled at room temperature with a magnetic thrilling bar to obtain a homogeneous and clear solution. The resulting solutions were then allowed to stand for two hours at room temperature without thrilling to digest the bubbles in the solution. Afterward, the resulting viscous solutions were electrified using an electrospinning device according to the conditions presented in Table 1.

**5. Preparation of Thin-film Composite**

The water-based solution and organic solution were arranged as follows: the water-based solution was prepared with 2%MPD and 2% TEA. To prepare the organic solution, 0.30 g of TMC was added into a 500-ml round-bottom flask supplied with a magnetic thrilling bar in an $N_2$ atmosphere, and thereafter 299.70 g n-hexane was added into the flask and the solution was stirred for 25 min. The prepared electrospun membranes were first taped to a glass plate using adhesive tape and then dipped in a bath with 250 ml of a water-based solution. After 1 h, electrospun membranes were taken out and the overload aqueous phase on the membrane surface was eliminated by rolling a rubber roller, and the organic solution was spilled on the surface of the membranes. After 60 s, the remaining organic solution on the surface of the membranes was eliminated and the resulting membrane was rinsed with DI water multiple times and preserved in DI water.

**6. Membrane Performance**

Water flux and desalination flux values were measured using a dead-end cell [21]. The effective membrane area in the present study was 12.57 cm$^2$. Using a gas regulator, the effective pressure on the membrane was set at seven bars. In all rejection tests, the aqueous solution of different salts with a concentration of 2,000 ppm was used as feed and every two hours the remaining solution in the cell from the previous time was drained; the feed solution was supplied from the main source to continue the rejection test. The passing flux was calculated by the following equation:

$$J = \frac{V}{A \times \Delta t}$$

where J is water flux, V is the quantity of permeate (L), A is the membrane effective (m$^2$), and Δt is the sampling time (h). The equation below was used to calculate the rejection.

$$R\% = 1 - \frac{C_p}{C_f} \times 100$$

where R is $C_p$ and $C_f$ are the salt concentration of collected permeate and the initial solution feed, respectively. Salt concentration was determined with a conductivimeter (Milwaukee-EC59-conductivimetro, Italy).

**7. Characterization of ENMs**

ENMs' morphology was studied using a scanning electron microscope (SEM, LEO 1455 VP, England) after gold plating and at an acceleration voltage of 10 kV. To measure the amount of hydrophilicity of the membranes, the static water contact angle was determined by a contact angle analysis system (OCA 15 plus; Dataphysics GmbH, Filderstadt, Germany) [22]. For each specimen, a 5 µl droplet of water as the probe liquid was administrated on the surface of the membrane in five various areas and the contact angle was measured by averaging the data. The porosity of the nanofibrous membranes was calculated by determining the amount of isopropyl alcohol adsorbed by the membranes continued by calculating as the equation below [23].

$$\text{Porosity}\% = \frac{W_w - W_d}{A \times l \times d \text{ isopropyl alcohol}} \times 100$$

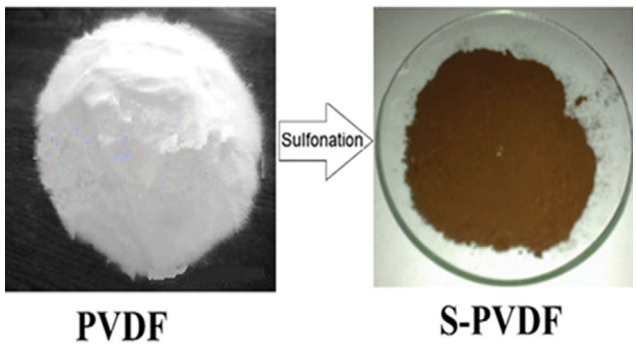


**Fig. 1. VDF and S-PVDF powder photograph.**

Herein, the description of symbols is as follows: $W_w$: The weight of the moisten membrane (g); $W_d$: The weight of dry membranes (g); A: The membrane area ($cm^2$); *l*: The membrane width (cm); d isopropyl alcohol: Density of isopropyl alcohol (0.786 g $cm^{-3}$).

The diameter of fibers (with measurements of 50 randomly chosen fibers) and surface pore diameter of membranes were examined through the SEM images by an image processing software, ImageJ (NIH, USA).

## RESULTS AND DISCUSSION

### 1. Proof of the Synthesis of Sulfonated Polyvinylidene Fluoride

Fig. 1 shows polyvinylidene fluoride powder and sulfonated polyvinylidene fluoride powder. As can be seen, the color of the powder changes from white to brown. To prove sulfonated polymer (figure out the sulfonation site), the analysis of $^1$H-NMR spectra was driven as outlined in Fig. 2. The $^1$H-NMR spectrum of intact PVDF exhibits two peaks in 2.22 ($H_a$) and 2.85 ($H_b$) ppm that are attributed to head-to-head (H-H) and head-to-tail (H-T) bonding arrangements. A new peak was discovered at 6.24 ppm after sulfonation (related to the hydrogen connected to the sulfonated carbon), and its existence proved that one of them had been replaced by the sulfonic acid group. It is assumed that the advent of some new peaks (the yellow rectangle) is due to the occurrence of adverse reactions over the course of the sulfonated reaction.

To prove the presence of a functional group ($SO_3H$) on PVDF

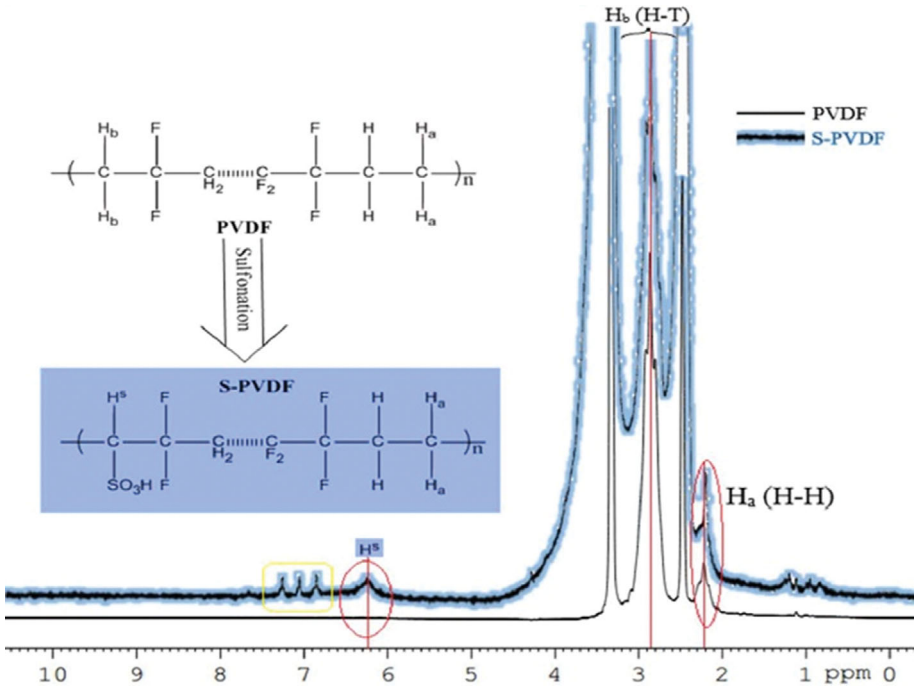


**Fig. 2. The $^1$H NMR spectrum of net PVDF and S-PVDF.**

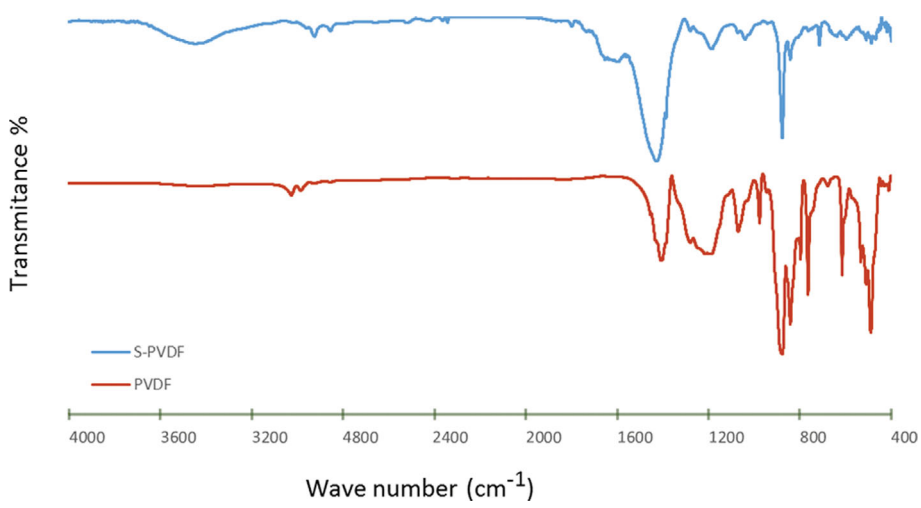


**Fig. 3. The FTIR spectrum of net PVDF and S-PVDF.**

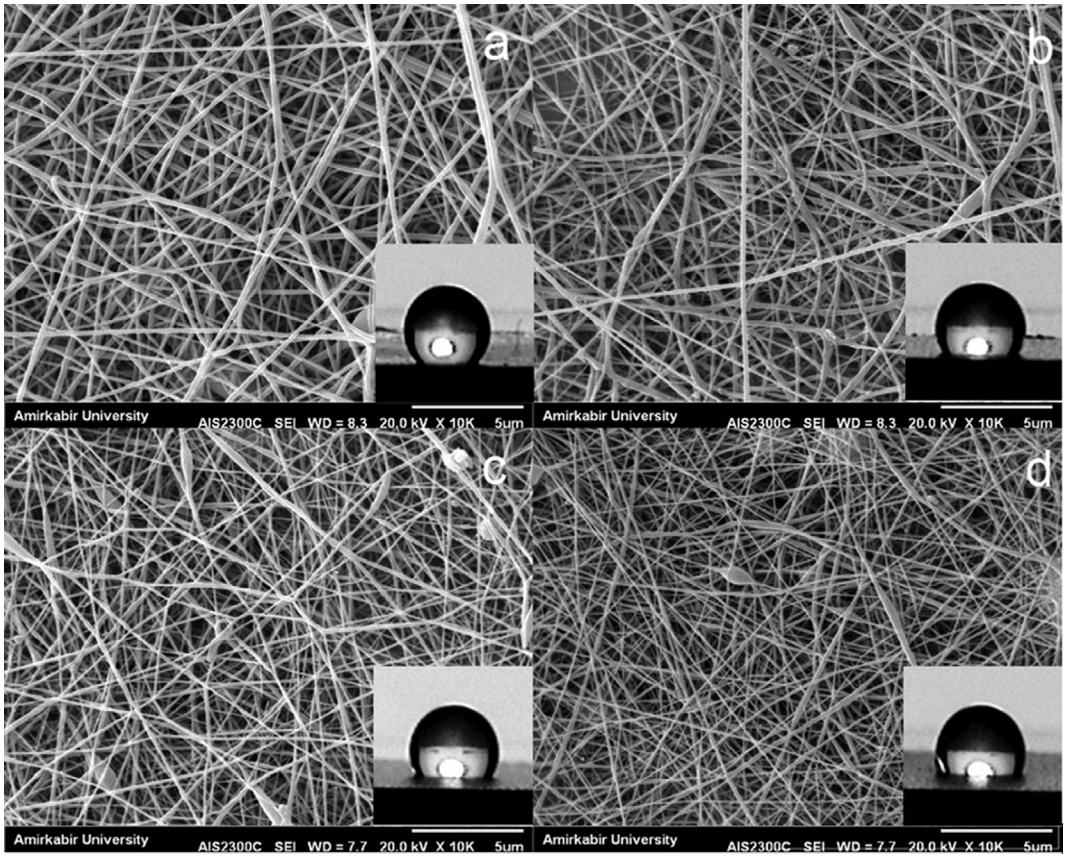


**Fig. 4. SEM images and water contact angle; (a) intact PVDF, (b) S-PVDF/PVDF (10/90), (c) S-PVDF/PVDF (30/70), and (d) S-PVDF/PVDF (50/50).**

polymer chains, the FT-IR spectra of PVDF and S-PVDF samples in the range of 4,000-400 $cm^{-1}$ were investigated and the results are presented in Fig. 3. By comparing these two spectra, new peaks appear for S-PVDF at 3,420 $cm^{-1}$, corresponding to the hydroxyl bonds of sulfonic acid groups, and 1,047 $cm^{-1}$, which are attributed to the symmetric tensile vibration of $SO_3H$ [24-26]. The asymmetric tensile vibrations of the $SO_3H$ group should be in 1,183 $cm^{-1}$ appear, but due to the overlap of the absorption of the main PVDF chain groups at this wavelength are not easily observable; however, it can be concluded that $SO_3H$ groups have been added [25].

**2. Morphology and Water Contact Angle of Nanofibers**

Fig. 4 shows the SEM images and water contact angle of nanofibers: (a) intact PVDF, (b) S-PVDF/PVDF (10/90), (c) S-PVDF/PVDF (30/70), and (d) S-PVDF/PVDF (50/50). As can be seen, the surface of the fibers is relatively smooth, without knots and drops. The contact angle of water can indicate any change in the hydrophilicity of the membrane [27], and the lower the value, the more hydrophilic the membrane [28]. It is obvious that with increasing the percentage of S-PVDF, the contact angle decreased, which indicates an increase in the hydrophilicity of the nanofibers. Although the backbone of S-PVDF is composed of a hydrophobic structure, the hydrophilic sulfonic acid groups, and the hydrophilic ion clusters are responsible for the hydrophilicity of S-PVDF. This effect leads to a decrease in the contact angle.

The following figure shows the numerical value of the contact angle for the membranes. Increasing the amount of S-PVDF in the composition increases the hydrophilicity of the membrane surface and thus reduces the contact angle [24]. As shown in Fig. 5, the contact angle of 137.1 degrees for intact PVDF nanofiber membranes was reduced to 117.2, 110.8, and 85.5 degrees for (10/90), (30/70), and (50/50) S-PVDF/PVDF, respectively.


**Fig. 5. Water contact angle of intact PVDF, SPVDF/PVDF (10/90), S-PVDF/PVDF (30/70), AND S-PVDF/PVDF (50/50).**

**3. Porosity of Nanofibers**

High porosity means higher membrane permeability. Fig. 6 shows the percentage of membrane porosity, and it is clear that the porosities of all membranes are almost equal. The uniformity of the poros-

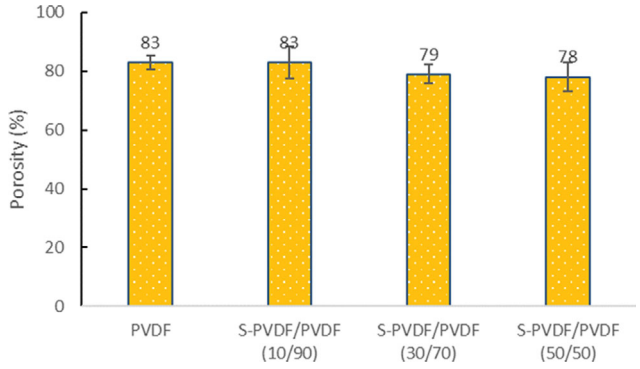


**Fig. 6. Porosity of nanofibers intact PVDF, S-PVDF/PVDF (10/90), S-PVDF/PVDF (30/70), and S-PVDF/PVDF (50/50).**

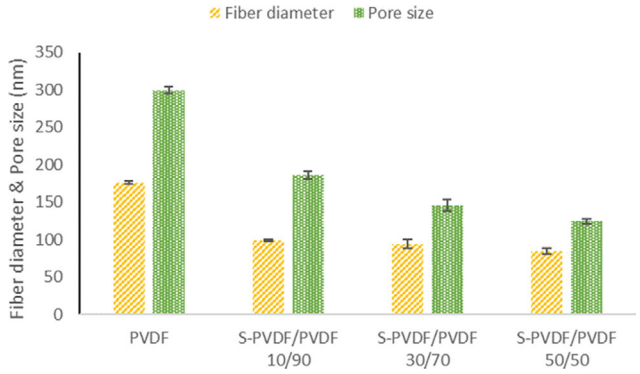


**Fig. 7. Nanofiber diameter and Pore size of intact PVDF, S-PVDF/PVDF (10/90), S-PVDF/PVDF (30/70), and S-PVDF/PVDF (50/50).**

ity facilitates the comparison between the membranes in terms of the sulfonation in the flux.

**4. Nanofiber Diameter and Pore Size**

To calculate the average diameter of electrospun nanofibers and pore size, Image-J and SPSS software were used. First, using Image-J, 80 fibers and 80 pores were randomly selected from SEM images and their diameter and size were determined. Then, using SPSS, the average diameter of nanofibers and the average pore size were calculated. Fig. 7 shows the average fiber diameter and the average pore size for intact PVDF, S-PVDF/PVDF (10/90), and S-PVDF/PVDF (30/70), and S-PVDF/PVDF (50/50) membranes prepared under the same electrospinning conditions. As can be seen, under the same conditions, the average fiber diameter has decreased from 177.56 for PVDF to 84.62 nm for S-PVDF/PVDF (50/50), which is due to the strong conductivity of the $SO_3H$ functional group. The polar functional group increases the conductivity of the electrospinning solution and reduces the diameter of fibers. It has been found that the size of the pores also decreases as the diameter of the fibers decreases. In the PVDF nanofibers with an average diameter of 176.07 nm, pores with an average size of 299.3 nm have been created, but in the S-PVDF/PVDF (50/50), with a decrease in the average fiber diameter to 84.62 nm, the size of the pores drops to 124.45 nm. It can be concluded that the reduction of pore size is due to the increase of the $SO_3H$ group in the solution [29].

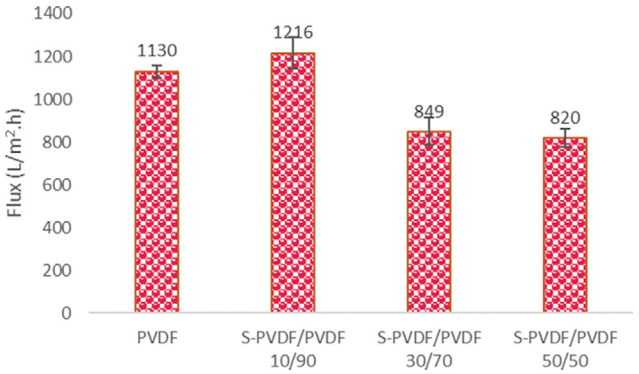


**Fig. 8. Flux ($l/m^2 \cdot h$) of intact PVDF, S-PVDF/PVDF (10/90), S-PVDF/PVDF (30/70), AND S-PVDF/PVDF (50/50).**

**5. Effect of Sulfonation on the Flux of Membranes**

To determine the effect of sulfonation, the flux for four intact PVDF, S-PVDF/PVDF (10/90), S-PVDF/PVDF (30/70), and S-PVDF/PVDF (50/50) at 0.5 bar pressure was calculated, and the results of which are presented in Fig. 8. As can be seen, the flow rate decreased from S-PVDF/PVDF (10/90) to S- PVDF/S-PVDF (50/50). While according to Fig. 5 the water contact angle for S-PVDF/PVDF (50/50) is less than the other two membranes due to the increase in the share of hydrophilic S-PVDF groups, and the S-PVDF/PVDF (50/50) was expected to have a higher flux than the two other membranes S-PVDF/PVDF (10/90) and S-PVDF/PVDF (30/70). Surprisingly, the results reveal that the S-PVDF/PVDF (50/50) membrane has a lower flux. We suggest that the reason behind this phenomenon is the reduction in the average fiber diameter from S-PVDF/PVDF (10/90) to S-PVDF/PVDF (50/50), and it will reduce the pore size and thus decrease the flux passing through the membrane. The S-PVDF/PVDF (10/90) membrane has a higher flux than PVDF due to the presence of 10% S-PVDF, which leads to an increase in hydrophilicity. However, as mentioned, higher percentages of S-PVDF, despite their higher hydrophilicity, cause a reduction in the pore sizes, and the smaller pore size of the nanofibers is the main reason for the lower flux.

**6. Examination of Composite Membrane: Proof of Polyamide Formation Using FT-IR**

Based on the SEM images in Fig. 9, a thin film composite was formed on the surface of support layers, and it was perfect and defect-free. Figs. 10 and 11 show the polymerization reaction between MPD and TMC and the formation of cross-linked polyamide and the FT-IR spectrum of monomer and the resulting polyamide. Peak A at $1{,}757^{-1}$ belongs to the carbonyl group of TMC. This peak appears at lower wavenumbers after polymerization (peak B at $1{,}653^{-1}$). Also, there is another small peak for carbonyl of carboxylic acid due to the hydrolysis after polymerization (peak C at $1{,}734^{-1}$). Peaks D at around $2{,}920^{-1}$ in all three spectra correspond to the C-H bonds of the aromatic ring. Two peaks of E at $3{,}322^{-1}$ and $3{,}387^{-1}$ correspond to the first type amine (MPD).

**7. Flux and Rejection**

To evaluate membranes, filtration tests were carried out for an extended time under a 5.0 bars pressure regulated by a nitrogen cylinder. First, the filtration process used deionized water. The pure water flux was determined in the early filtration stage of all mem-

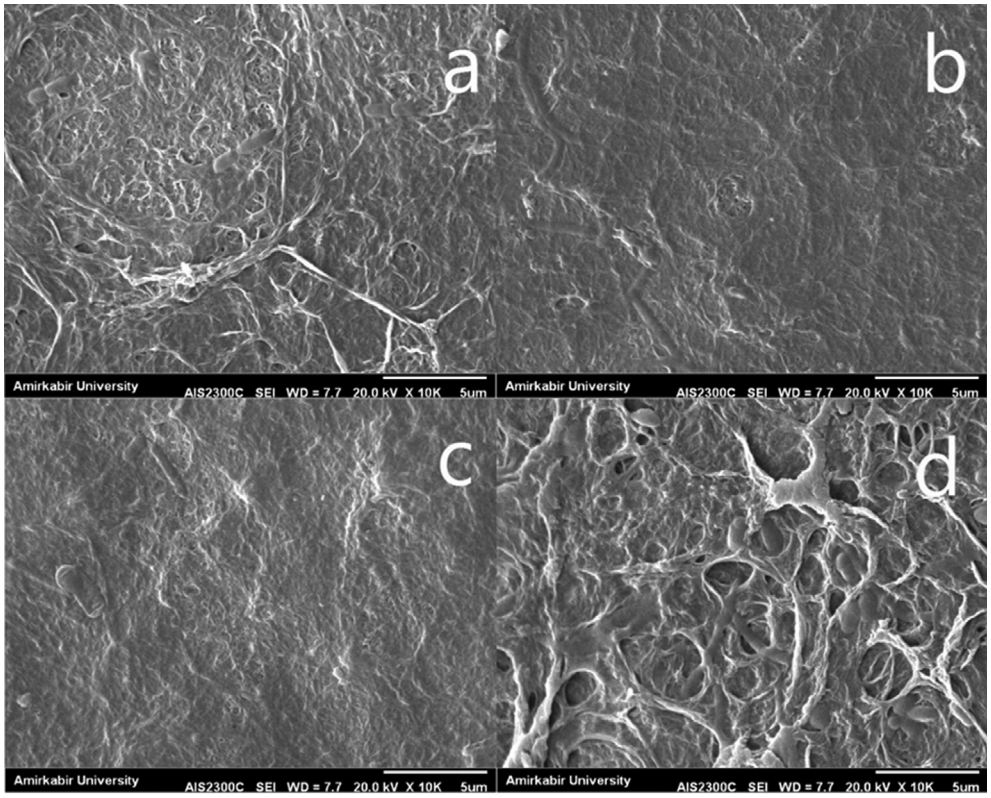


**Fig. 9. SEM images of thin film composite on supports; (a) intact PVDF, (b) S-PVDF/PVDF (10/90), (c) S-PVDF/PVDF (30/70), and (d) S-PVDF/PVDF (50/50).**

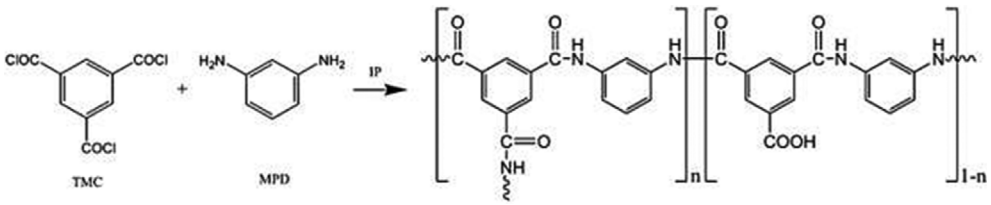


**Fig. 10. Cross-linked polyamide.**

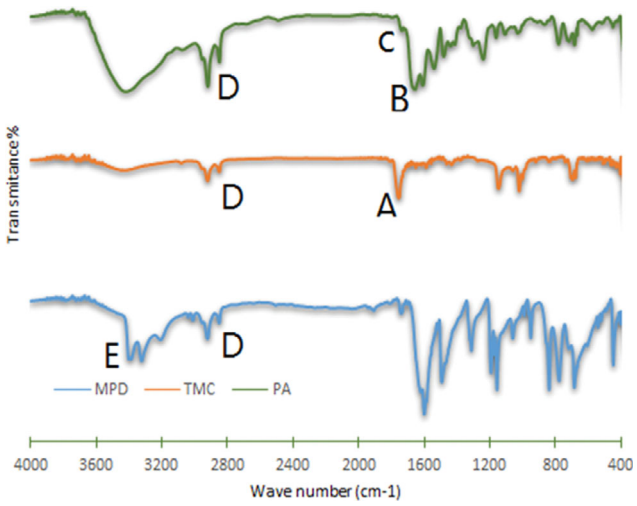


**Fig. 11. The FTIR spectrum of MPD, TMC, and the resulting polyamide.**

branes until all of them reached a steady state. Fig. 12 shows the pure water flux of membranes for 90 minutes. Hydrophilicity, pore size, and nanofiber diameter play a critical role in the formation of a thin polyamide layer on the support surface. So that on hydrophilic surfaces, this layer is formed better and denser. Also, the smaller fibers and pores of the support lead to a denser thin layer, and as a result, the flux will decrease and this trend is visible with the increasing percentage of S-PVDF. In addition to the properties of the thin-film layer, the support layer should let the solution pass through. Hence, there is a wide range of properties that affect the flux of different asymmetric membranes. We noticed that after reaching a steady-state the membrane containing 10% S-PVDF had the highest flux by 25.5 $L/m^2 \cdot h$, and the flux was reduced by increasing S-PVDF. It is interesting that the PVDF-based membrane had a higher flux compared to membranes containing 50% S-PVDF. In this study, different percentages of S-PVDF were added to the electrospinning solution and caused boosted hydrophilicity. In addition, increasing S-PVDF decreased the viscosity and height-

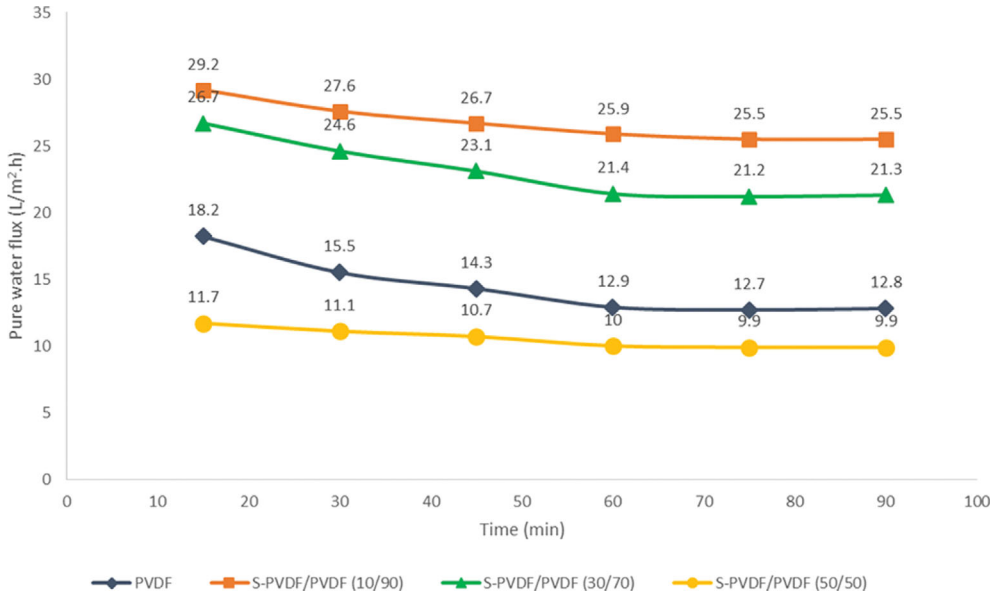


**Fig. 12. Pure water flux of membrane by time in 90 min.**

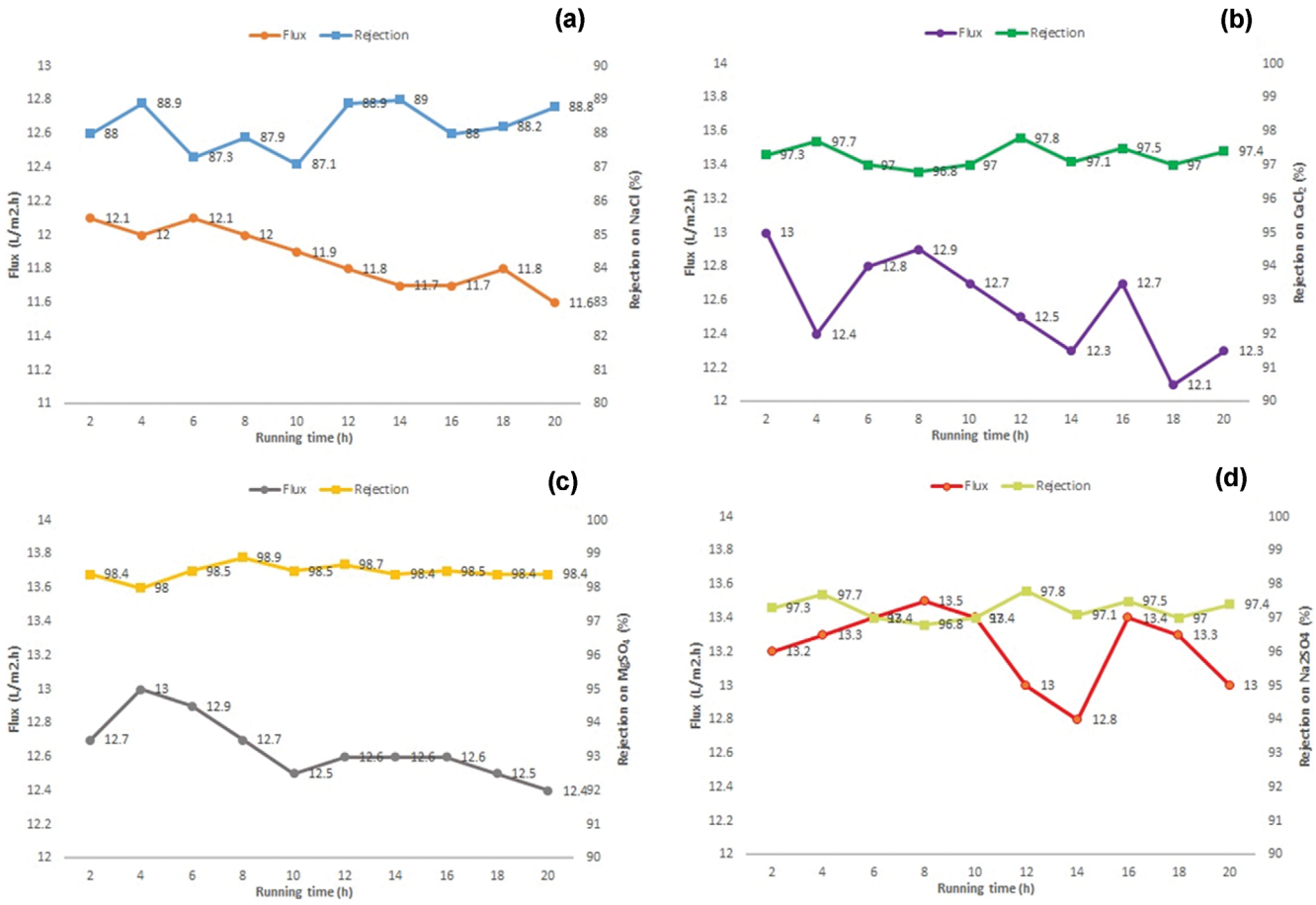


**Fig. 13. Flux & Rejection of 10% S-PVDF membrane using different solutions (a) NaCl, (b) $CaCl_2$, (c) $MgSO_4$, (d) $Na_2SO_4$.**

ened the electrical conductivity of the electrospinning solution, and ultimately reduced the diameter of the fibers. The presence of these properties in the support causes the formation of a uniform polyamide layer and changes the flux and salt rejection. The resulting composite membrane on the support containing 10% S-PVDF had higher flux and rejection and was selected as the optimal mem-

**Table 2. Flux of 10% S-PVDF membrane using different solutions**

| Flux ($l/m^2 \cdot h$) \ Time (h) | 2 | 4 | 6 | 8 | 10 | 12 | 14 | 16 | 18 | 20 |
|---|---|---|---|---|---|---|---|---|---|---|
| NaCl | 12.1 | 12.1 | 12.1 | 12.1 | 12.1 | 12.1 | 12.1 | 12.1 | 12.1 | 12.1 |
| $CaCl_2$ | 13 | 13 | 13 | 13 | 13 | 13 | 13 | 13 | 13 | 13 |
| $MgSO_4$ | 12.7 | 12.7 | 12.7 | 12.7 | 12.7 | 12.7 | 12.7 | 12.7 | 12.7 | 12.7 |
| $Na_2SO_4$ | 13.2 | 13.2 | 13.2 | 13.2 | 13.2 | 13.2 | 13.2 | 13.2 | 13.2 | 13.2 |

**Table 3. Rejection of 10% S-PVDF membrane using different solutions**

| Rejection (%) \ Time (h) | 2 | 4 | 6 | 8 | 10 | 12 | 14 | 16 | 18 | 20 |
|---|---|---|---|---|---|---|---|---|---|---|
| NaCl | 88 | 88.9 | 87.3 | 87.9 | 87.1 | 88.9 | 89 | 88 | 88.2 | 88.8 |
| $CaCl_2$ | 97.3 | 97.7 | 97 | 96.8 | 97 | 97.8 | 97.1 | 97.5 | 97 | 97.4 |
| $MgSO_4$ | 98.4 | 98 | 98.5 | 98.9 | 98.5 | 98.7 | 98.4 | 98.5 | 98.4 | 98.4 |
| $Na_2SO_4$ | 97.3 | 97.7 | 97 | 96.8 | 97 | 97.8 | 97.1 | 97.5 | 97 | 97.4 |

brane and its rejection was tested using several other salts.

After the steady-state of the 10%, the S-PVDF-based membrane was quantified according to pure water; feed solution tests were done for a prolonged time. Four types of inorganic compounds, that is, NaCl, $CaCl_2$, $MgSO_4$, and $Na_2SO_4$, were selected for the feed solution and the concentration of all solutions was 2,000 ppm. The filtering application of the four types of solution is demonstrated in Fig. 13 and their details are briefed in Tables 2 and 3. In Fig. 13, flow performance across all solutions shows a slight downward trend. This may be due to concentration polarization caused by the use of a dead-end filter cell. A precise amount of feed solution was employed in each experiment, and the feed solution could not circulate through the dead-end filtration system. As the water molecules pass through the membrane, the salt ions are locked up and the concentration of the feed solution continues to grow. Considering that the fraction of salt ions rises quickly, concentrated feed solutions gather on the surface of the membrane and generate salt discharge or fouling. Furthermore, the osmotic pressure rises proportionally to the concentration of the feed source and, consequently, the flow of water tends to decrease over filtration. Finally, the 10% S-PVDF membrane exhibited a strong rejection performance for bivalent salts. The rejection mechanism in nanofiltration membranes does not only depend on the size of pores and ions but also follows complex mechanisms such as Donnan exclusion, which involves factors such as ion charges and membrane surface charge. However, few studies have been done on the complex process of rejection and it is still not fully known. Based on Donnan exclusion principles, the rejection of ions improves with a higher charge of co-ions and falls with a higher counter-ion charge. Nanofiltration membranes can be considered as negatively charged surfaces, and one of the effective factors in this surface charge is functional groups such as sulfonic acid in the membrane in the present study [20]. Past research has shown that the order of salt rejection in negatively charged membranes is $Na_2SO_4$>$MgSO_4$>$MgCl_2$>$CaCl_2$>NaCl. However, deviations from this order have been observed, thus requiring more detailed studies and models to answer them [30]. The rejection rates of bivalent salts were higher than 97% and were about 88% for univalent salt.

## CONCLUSION

A thin-film composite membrane from MPD and TMC was prepared on the surface of a recently developed electrospun nanofibrous scaffold from sulfonated PVDF manufactured by the electrospinning approach. The $^1$HNMR and FT-IR techniques confirmed sulfonation of PVDF, and based on previous experience the electrospun mats were fabricated using different percentages of S-PVDF. The resulting SEM showed that electrospuns were smooth without beads or droplets; they also proved the formation of polyamide thin film on the surface of electrospun membranes. FT-IR techniques confirmed polymerization between monomers MPD and TMC. Addition of S-PVDF heightened the electrical conductivity of the electrospinning feed and ultimately reduced the diameter of fibers and pore size of the ENMs. Sulfonation of PVDF caused the thin film to adhere to electrospun membranes well and rise in the hydrophobicity and the water flow compared to the intact PVDF nanofibrous membrane. Among the various membranes (10, 30, and 50), the membrane with 10% represented the highest pure water flux. The results of S-PVDF/PVDF (10/90) illustrated rejection of higher than 97% for bivalent salts and around 88% for univalent salt.

## COMPETING INTERESTS

There is no conflict of interest to declare.

## REFERENCES

1. G. A.Tularam and M. Ilahee, *J. Environ. Monit.*, **9**, 805 (2007).
2. R. W. Baker, *Membrane technology and applications*, John Wiley & Sons (2012).
3. O. Kutowy and S. Sourirajan, *J. Appl. Polym. Sci.*, **19**, 1449 (1975).
4. T. J. Sill and H. A. Von Recum, *Biomaterials*, **29**, 1989 (2008).
5. S. Chew, Y. Wen, Y. Dzenis and K. W. Leong, *Curr. Pharm. Des.*,

**12**, 4751 (2006).
6. Z.-M. Huang, Y.-Z. Zhang, M. Kotaki and S. Ramakrishna, *Compos. Sci. Technol.*, **63**, 2223 (2003).
7. D. Reneker, A. L. Yarin, E. Zussman and H. Xu, *Adv. Appl. Mech.*, **41**, 43 (2007).
8. X. Zhang, M. R. Reagan and D. L. Kaplan, *Adv. Drug Deliv. Rev.*, **61**, 988 (2009).
9. O. Qanati, A. Ahmadi, M. S. Seyed dorraji, M. H. Rasoulifard and V. Vatanpour, *Polym. Bull.*, **75**, 3407 (2018).
10. Y. Mansourpanah, S. Madaeni and A. Rahimpour, *J. Membr. Sci.*, **343**, 219 (2009).
11. M. Safarpour, A. Khataee and V. Vatanpour, *J. Membr. Sci.*, **489**, 43 (2015).
12. L. Shen, C. Cheng, X. Yu, Y. Yang, X. Wang, M. Zhu and B. S. Hsiao, *J. Mater. Chem. A*, **4**, 15575 (2016).
13. F. Soyekwo, Q. Zhang, R. Gao, Y. Qu, C. Lin, X. Huang, A. Zhu and Q. Liu, *J. Membr. Sci.*, **524**, 174 (2017).
14. S. S. Ray, S.-S. Chen, C.-W. Li, N. C. Nguyen and H. T. Nguyen, *RSC Adv.*, **6**, 85495 (2016).
15. Y. Yang, X. Wang and B. Hsiao, IOP Conference Series: *Mater. Sci. Eng.*, **137**, 012047 (2016).
16. M. Tian, C. Qiu, Y. Liao, S. Chou and R. Wang, *Sep. Purif. Technol.*, **118**, 727 (2013).
17. J. Wang, P. Zhang, B. Liang, Y. Liu, T. Xu, L. Wang, B. Cao and K. Pan, *ACS Appl. Mater. Interfaces*, **8**, 6211 (2016).
18. V. Vatanpour, M. Esmaeili and M. H. Davood Abadi Farahani, *J. Membr. Sci.*, **466**, 70 (2014).
19. G. N. B. Baroña, B. J. Cha and B. Jung, *J. Membr. Sci.*, **290**, 46 (2007).
20. A. Ahmadi, O. Qanati, M. S. Seyed Dorraji, M. H. Rasoulifard and V. Vatanpour, *J. Membr. Sci.*, **536**, 86 (2017).
21. H. J. Kim, K. Choi, Y. Baek, D.-G. Kim, J. Shim, J. Yoon and J.-C. Lee, *ACS Appl. Mater. Interfaces*, **6**, 2819 (2014).
22. J. Wagner, *Membrane filtration handbook: Practical tips and hints*, Osmonics Inc., Minnesota U.S.A. (2001).
23. J. Ding, Y. Kong, P. Li and J. Yang, *J. Electrochem. Soc.*, **159**, A1474 (2012).
24. H. Farrokhzad, T. Kikhavani, F. Monnaie, S. N. Ashrafizadeh, G. Koeckelberghs, T. Van Gerven and B. Van der Bruggen, *J. Membr. Sci.*, **474**, 167 (2015).
25. H. Ma, C. Burger, B. S. Hsiao and B. Chu, *J. Mater. Chem.*, **21**, 7507 (2011).
26. I. C. Kim, J. G. Choi and T. M. Tak, *J. Appl. Polym. Sci.*, **74**, 2046 (1999).
27. S. S. Homaeigohar and M. Elbahri, *J. Colloid Interface Sci.*, **372**, 6 (2012).
28. S. Zinadini, A. A. Zinatizadeh, M. Rahimi, V. Vatanpour and H. Zangeneh, *J. Membr. Sci.*, **453**, 292 (2014).
29. W. Jang, J. Yun, K. Jeonb and H. Byun, *RSC Adv.*, **5**, 46711 (2015).
30. N. S. Suhalim, N. Kasim, E. Mahmoudi, I. J. Shamsudin, A. W. Mohammad, F. M. Zuki and N. L.-A. Jamari, *Nanomaterials*, **12**, 437 (2017).